



Influence of natural and synthetic blended polymers on the electrospun PVA/chitosan/PANI composite nanofibers to be used for dye decolorization

M.A. Khalil^a, M.F. El-Kady^{b,c}, G.M. El-Subruiti^a, E.M. El-Sayed^{b,*}

^aFaculty of Science-Alexandria University, Advanced Technology and New Materials Research Institute (ATNMRI), City of Scientific Research and Technological Applications, emails: mohammedali@alexu.edu.eg (M.A. Khalil), gehanmsubruiti@alexu.edu.eg (G.M. El-Subruiti)

^bFabrication Technology Research Department, Advanced Technology and New Materials Research Institute (ATNMRI), City of Scientific Research and Technological Applications, Tel. 01227155270; email: mdr.eman@yahoo.com (E.M. Mohamed El-Sayed)

^cChemical Engineering - Chemical and Petroleum Engineering Department Egypt-Japan University of Science and technology (E-JUST), email: Marwa.f.elkady@gmail.com (M.F. El-Kady)

Received 29 June 2019; Accepted 3 November 2019

ABSTRACT

In this work, mixing polyvinyl alcohol (PVA), chitosan (CS) and polyaniline (PANI) to prepare composite nanofibers with improved adsorption capacity using electrospinning technique has been studied, thereby overcoming the difficulty of producing PANI nanofibers. The morphologies of the prepared nanocomposites were fully examined by SEM, Fourier transform infrared spectroscopy and X-ray diffraction measurements. Results indicated that the blended PVA/CS/PANI-based nanofibers exhibited better size morphology with smaller diameter than (PVA/PANI) and pure polyaniline. Batch experiments were conducted using the prepared (PVA/PANI/CS) composite to study its affinity for dye decolorization. Different factors affecting the adsorption process such as contact time, initial dye concentration, temperature and pH were optimized. The maximum percentage removal was found to be 96% at 300 rpm using adsorbent dose of 60 mg and temperature of 25°C and initial dye concentration 50 ppm. Also, the adsorption isotherms, kinetics and thermodynamics for the removal process were studied. The adsorption process followed Freundlich isotherm and pseudo-first order kinetics.

Keywords: Electrospinning; Polyaniline; Chitosan; Polyvinyl alcohol; Nanofibers

1. Introduction

Dyes are common hazardous contaminants that can cause detrimental effects on environment and natural water sources. Hence, the removal of these organic pollutants from water system is a priority for ensuring a safe and clean environment. From the view point of simplicity and economy, the acid dyes such as acid blue 25 removal is difficult because of the complexity of aromatic structure as well as the synthetic origin of these contaminants [1,2]. Thus, for the removal of such dyes from aqueous mediums, efficient treatment

procedures are required; they tend to pass through the traditional treatment [3]. Adsorption has become the most widely used technology for simultaneous water deep purification [4–6]. Adsorption processes have many applications for the removal and recovery of metals, dyes, oils, organic mixtures and pharmaceuticals from water [7], with the gradual developments of new adsorbent materials, the field of adsorption became broader and specific in nature for particular pollutants including heavy metals, phenols, antibiotics, and pesticides [8]. Among the various adsorbents, polyaniline (PANI) containing plenty amount of positively charged amine and imine groups has drawn tremendous attention due to its ease

* Corresponding author.

of synthesis, low cost, remarkable environmental stability and reversibility [9,10]. Although natural polymers are more favored because of their natural occurring, biocompatibility and biodegradability [11], synthetic polymers have better thermal stability and mechanical properties [12–14]. Thus, blending synthetic polymers such as polyaniline and polyvinyl alcohol with natural polymer such as chitosan may form a polymeric composite with physical and chemical properties compared with those of single components [12]. The advanced nanocomposites play an important role in the environmental protection due to their specificity, selectivity, and a wide range of usability; great efforts have been done to improve the chemical, mechanical, and thermal stabilities of composites so they can be used as a selective material for removal of heavy metals and dyes [15]. Nanofibers produced by electrospinning have attracted growing interests for biological and chemical separations. Electrospinning is a processing technique in which an electrically charged jet of polymer solution is captured on a grounded collector plate. The electrical charge of the polymer solution allows the polymer to form uniform and very thin fibers, commonly known as electrospun nanofibers. The electrospinning process results in a product with a high surface area-to-volume ratio, which makes it ideal for many applications [16,17]. Some of the many uses of electrospun nanofibers include as adsorbents for protein purification [18,19], as scaffolds for tissue engineering [20], in nanocomposites, in materials for fuel cells, solar cells, Li-ion batteries, and supercapacitors [21] and in water treatment in the form of non-carbonized filtration membranes [22]. Electrospun nanofiber membranes can be used as either an adsorbent material [23]. In this work, different polyaniline mixtures with polyvinyl alcohol (PVA) or chitosan (CS)/PVA were electrospun to produce nanofibers (NFs). The influence of blending different polymers was studied and optimized based on SEM images of the produced nanofibers. Batch experiments were conducted using the best prepared composites to study its efficiency for dye decolorization.

2. Materials and methods

2.1. Materials

Chloroform, glacial acetic acid, glutaraldehyde (25% aqueous solution), hydrochloric acid (37%), potassium dichromate and sodium hydroxide were purchased from Sigma-Aldrich, USA. Acid blue 25, ethanol, and N,N-dimethylformamide were obtained from Fisher Scientific, USA. Chitosan was obtained from Bio Basic Inc., Canada. Aniline monomer was purchased from Oxford Lab Chem, India. Polyvinyl alcohol (M.wt = 72,000 g/mol, Degree of polymerization 1,700–1,800) was obtained from Qualikems Fine Chemicals Pvt. Ltd., India.

2.2. Preparation of polyaniline nanoparticles (PANI)

Polyaniline nanoparticles were synthesized by oxidative polymerization of aniline monomer by using potassium dichromate as oxidizer according to the method of Zoromba et al. [24] with some modifications to simplify the preparation process and increasing the yield, where a mixture of 20 mL conc. HCl, 10 mL aniline monomer and 10 mL distilled water

were stirred vigorously for 15 min, then 50 mL of $K_2Cr_2O_7$ (0.44 M) solution was added to the mixture dropwise during vigorous stirring, then the total volume was completed to 100 mL by distilled water. The precipitated PANI was filtered and washed with ethanol and distilled water several times then dried at 60°C for 24 h in an oven.

2.3. Preparation of polyaniline nanofibers

Polyaniline nanofibers were prepared with electrospinning of pure polyaniline solution. 100 mg of polyaniline were dispersed in 10 mL chloroform. The solution was stirred for 6 h. The solution was then set on an electrospinning setup (NANON, Germany) to form the nanofiber on aluminum foil under a voltage of 35 kV. The working distance between nozzle to collector was 15 cm and the flow rate was 0.3 mL h⁻¹.

2.4. Preparation of PANI/PVA nanofibers

PANI/PVA nanofibers were prepared using direct electrospinning route. All the electrospinning parameters were optimized. In a typical synthesizer, three solutions of different PVA and PANI ratios were prepared by adding different amounts of PANI NPs to 5 wt.% PVA solution in a mixture of solvents (H₂O:DMF) (1:1). The mixture is vigorously stirred at 80°C for 1 h till obtaining clear viscous solution then cooled to room temperature, three different amounts of PANI NPs (0.5, 1, 2.5 wt.%) were added to the previous solution with stirring till a viscous homogeneous solutions was obtained. The precursor solution was set on an electrospinning setup for nanofiber formation under a voltage of 35 kV. PANI/PVA nanofibers were collected on aluminum foil with a nozzle to collector distance of 15 cm and a flow rate of 0.3 mL/h.

2.5. Preparation of (PVA/PANI/CS) nanofibers

Three solutions with different PVA, PANI and CS ratios were prepared by adding different amounts of PANI and CS to 5 wt.% solution of PVA in solvent mixture of (H₂O:DMF). 1.5 g of PVA was dissolved in 200 mL mixture of (H₂O:DMF) (1:1) by vigorous stirring at 80°C for 1 h till complete dissolution, three different amounts of PANI NPs (3.0, 6.0 and 6.0 g) were added to the previous PVA solution under stirring till a viscous homogeneous solution was obtained. Then different amounts of chitosan (3.0, 3.0 and 1.5 g) were dissolved in 100 mL 3% acetic acid solution in distilled water by vigorous stirring at 80°C for 1 h. The chitosan solutions were mixed with the previously prepared (PVA/PANI) solution, respectively. The precursor solution was set on an electrospinning setup for nanofiber formation under a voltage of 35 kV. PVA/PANI/CS nanofibers were collected on aluminum foil with a nozzle to collector distance of 15 cm and a flow rate of 0.3 mL/h.

2.6. Cross-linking of PANI-composites

Cross-linking is a must for hydrophilic polymers (PVA and CS) to decrease their solubility in water and increase their stability under extreme conditions of temperature, pH and pressure [25]. The cross-linking reaction of the polymeric

chains was carried out by adding 100 μL glutaraldehyde for each 100 mL of polymer solution with vigorous stirring at 60°C for 1 h. The solution was stored in refrigerator overnight before the electrospinning process [26].

2.7. Measurements and characterization of the prepared nanofibers

The morphology of the prepared PANI nanoparticles and fabricated PANI-based nanofibers was determined by using SEM (JEOL JSM 6360LA, Japan). The X-ray diffraction (XRD) pattern of the samples was determined by X-ray diffractometer (Shimadzu-7000, Japan). The Fourier transform infrared spectroscopy (FTIR) spectra were determined by Fourier Transform Infrared Spectrophotometer (Shimadzu FTIR-8400 S, Japan). The thermal stability of the samples was studied by using Thermo Gravimetric Analyzer (Shimadzu TGA-50, Japan). Measurement of Brunauer–Emmett–Teller (BET) surface area was performed using N_2 adsorption/desorption isotherms using Belsorp II mini (BEL Japan Inc).

2.8. Batch adsorption for dye decolorization

The optimized PVA/CS/PANI composite nanofibers have been prepared with high thickness. A series of batch experiments were performed to study the removal of AB 25 using these nanofibers. The several processing parameters affecting the adsorption process, contact time, initial dye concentration, temperature and pH were studied, as well as studying the adsorption isotherms, kinetics and thermodynamics of the process have been considered. The initial and final dye concentrations for all solutions were measured using UV-Visible spectrophotometer (T70 single split beam), then the percentage of dye removal %R was calculated from the following equation:

$$\%R = \frac{C_0 - C}{C_0} \times 100 \quad (1)$$

where %R is the percentage of removal, C_0 and C are the initial and final dye concentrations (mg/L), respectively. The amount of dye adsorbed (q_t) at different time intervals (t) was determined from the following equation:

$$q_t = \frac{C_0 - C_t}{\frac{m}{V}} \quad (2)$$

where q_t (mg/g) is the adsorption capacity at time t , C_0 (mg/L) is the initial dye concentration, C_t (mg/L) is the dye concentration at time t , V (L) is the volume of the solution, and m (g) is the mass of PVA/CS/PANI nanofibers used [27].

3. Results and discussions

3.1. Electrospinning of PVA/PANI-based composite

No fibers are formed by the electrospinning of pure PANI solution; this is due to the low density of PANI polymer solution, where pure PANI cannot form true solution because it is partially dissolved and it is just dispersed well with other polymers to be electrospun [28]. So, another

polymer should be blended with PANI to obtain viscous polymer solution which can be electrospun easily. First, we blended PANI and PVA with different ratios. SEM images of the PANI-based composites nanofibers with different ratios of PVA to PANI (10:1), (5:1) and (2:1) are shown in Figs. 1a–c, respectively.

It was found that by increasing the concentration of PANI, the prepared nanofibers diameters decrease in addition to the decrease of beads number. But it was observed that by increasing the concentration of PANI to a certain amount, excess PANI nanoparticles were observed to be non-dispersed which restrict the electrospinning process due to block out of the syringe needle with time.

So, the optimum blending ratio of PVA/PANI is considered to be 5:1. As an attempt to decrease the diameter of the fabricated PANI composite nanofibers, the effect of adding another polymer has been investigated.

3.2. Electrospinning of PVA/CS/PANI composite

The SEM images of the PVA/CS/PANI nanofibers with different concentration ratios of PVA:PANI:CS 5:1:1, 5:2:1 and 5:2:0.5 are shown in Fig. 2, where the effect of PANI and CS concentrations can be explained. A uniform nanofiber that is free from beads with average diameter of 35 nm was fabricated at PVA:PANI:CS mixing ratio of 5:1:1 as illustrated from Fig. 2a. The increase of PANI concentration in the presence of chitosan increases the average diameter to about 49 nm as shown in Fig. 2b. As shown from Fig. 2c, the average nanofiber diameter was increased to about 87 nm that implies the negative effect of decreasing chitosan concentration.

All in all, adding chitosan to PANI-composites nanofibers decrease the diameters of the formed nanofibers and decrease the presence of beads. Also, chitosan has a great effect on improving the morphology of the nanofibers, in addition to making the electrospinning process easier. Also chitosan's functional groups and natural chelating properties make chitosan useful for the binding and removal of different types of water pollutants. Finally, the best prepared PANI-composite nanofibers were the nanofibers prepared by electrospinning of polymer solution with concentration ratio PVA:PANI:CS 5:1:1 at conditions of flow rate 0.3 mL/h, applied voltage 35 kV and travel distance 15 cm; this composite will be used for further studies.

3.3. Characterization of the best fabricated PANI-based composite nanofiber

3.3.1. Transmission electron microscope

As shown in Fig. 3, the transmission electron microscope (TEM) images show the SEM micrographs of the prepared PANI-composite. Nanofibers with the concentration ratio of PVA:PANI:CS 5:1:1.

3.3.2. X-ray diffraction

The XRD patterns of both PANI nanoparticles and the prepared optimum prepared fabricated electrospun nanofiber were compared as shown in Fig. 4, the XRD pattern

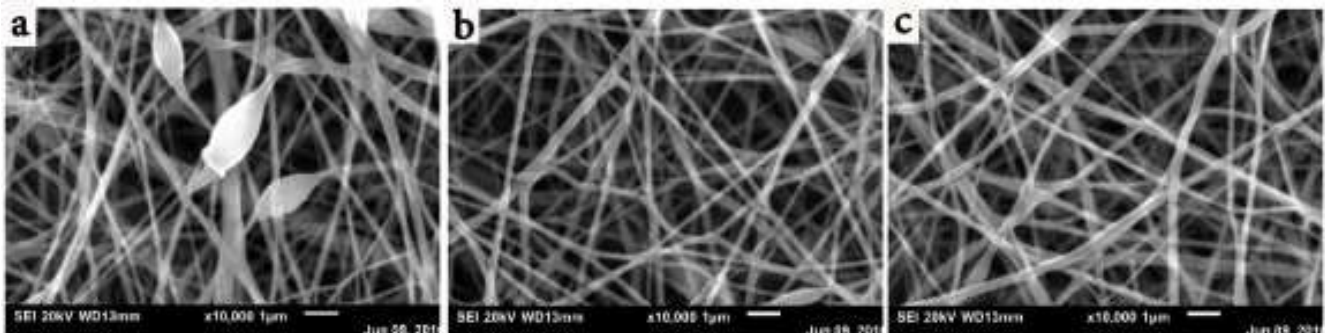


Fig. 1. SEM images of (PVA/PANI) composites nanofibers.

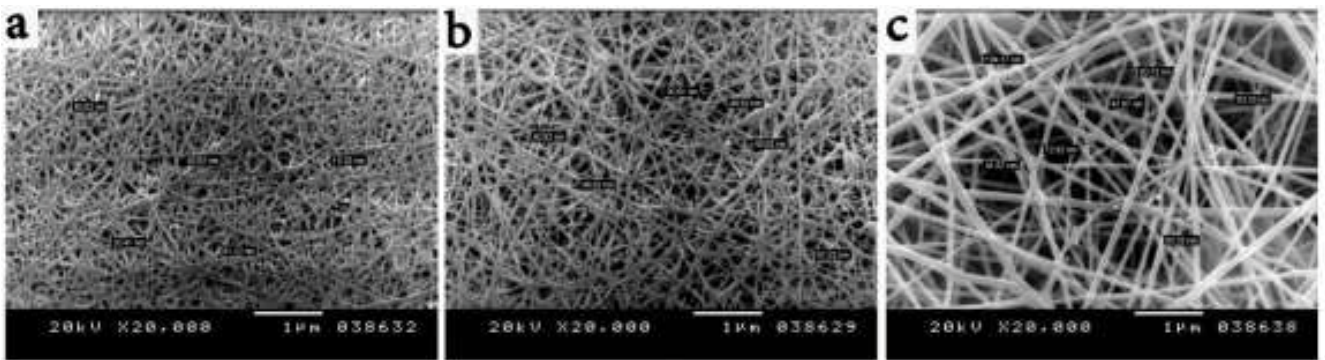


Fig. 2. SEM images of PVA/CS/PANI composites nanofibers with different concentration ratios of PVA:PANI:CS. (a) 5:1:1, (b) 5:2:1, and (c) 5:2:0.5.

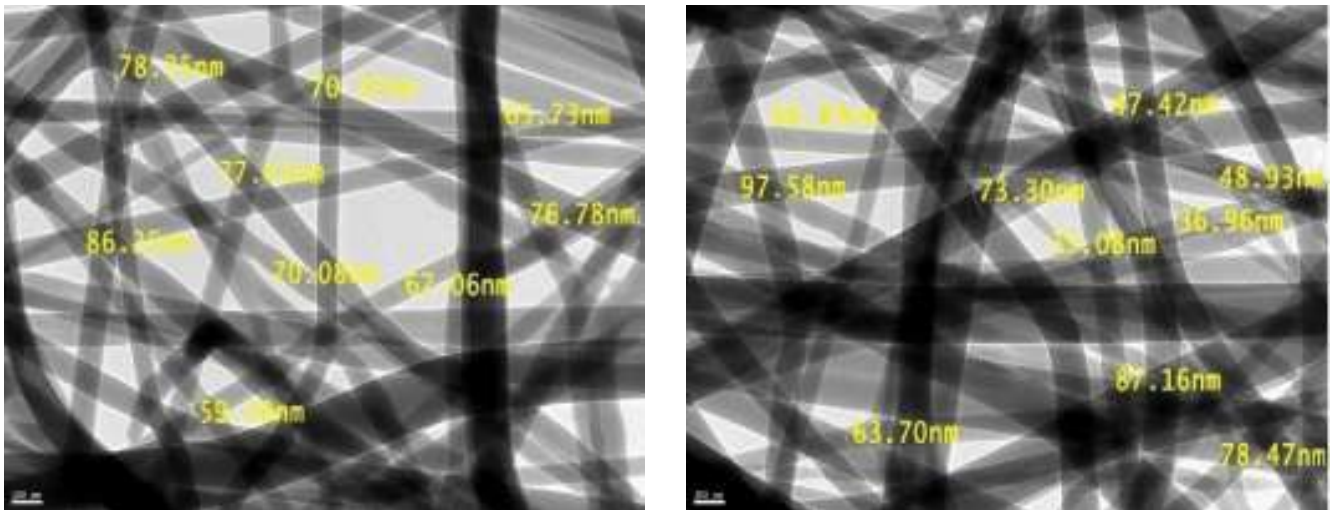


Fig. 3. TEM images of the optimized PANI-composite nanofibers with the concentration ratio of PVA:PANI:CS 5:1:1.

of the prepared polyaniline nanoparticles shows four sharp peaks at 2θ of 25.57° , 26.82° , 20.70° and 15.23° . This confirms the crystalline structure of the synthesized PANI due to planar nature of benzenoid and quinoid units in PANI chain [29]. The XRD pattern of the optimized PANI-based composite nanofibers shows three peaks at 2θ of 20.14° , 19.34° and 21.02° , which are corresponding to the characteristic peaks of chitosan [30,31], polyvinyl alcohol [30,32,33] and PANI, respectively. This XRD pattern confirms that the

PANI-composite nanofibers are less in crystallinity compared with the synthesized PANI nanoparticles due to the presence of PVA and CS [33], where chitosan is known as a partially crystalline polymer, and its crystalline nature exhibited due to the accumulation of linear chains in the structure of chitosan through inter-molecular and intra-molecular hydrogen bonding between hydroxyl and amino groups in chitosan [29,30], also polyvinyl alcohol is known by its semi crystalline nature [29,31,32].

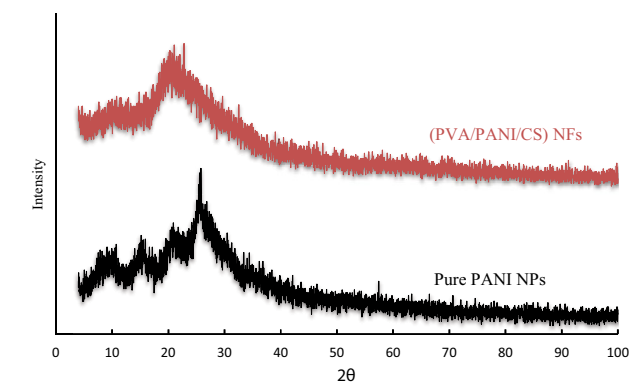


Fig. 4. XRD pattern of the prepared polyaniline nanoparticles and the optimized PANI-composite nanofibers.

3.3.3. Fourier transform infrared spectroscopy

FTIR spectrum of prepared PANI nanoparticles was compared with the spectrum of the optimum prepared PANI-based composite nanofiber in Fig. 5; the FTIR spectrum of pure PANI shows a prominent band at $3,435\text{ cm}^{-1}$ due to N–H stretching vibrations [30,34]. Another weak band is observed at $2,918\text{ cm}^{-1}$, which is located in the C–H stretching region, this band indicates the number of hydrogen atoms bonded to benzene ring during doping [35]. The main chain characteristic bands at $1,554$ and $1,458\text{ cm}^{-1}$ are attributed to the C=N and C=C stretching modes for the quinoid and benzenoid rings, respectively [20,26,27]. The band at $1,276\text{ cm}^{-1}$ is assigned to C–N stretching vibration [30,36,38]. There are another two bands; the first one at $1,114\text{ cm}^{-1}$ due to C–H in-plane bending vibration and the second band at 798 cm^{-1} is assigned to C–H out-of-plane bending vibration of 1,4-disubstituted benzene ring [31,37].

The FTIR spectra of PANI-based composite NFs are shown in Fig. 5; the figure shows a strong broad band at $3,300\text{--}3,500\text{ cm}^{-1}$, which is assigned to the stretching vibration of –OH and –NH₂ groups and the intermolecular hydrogen bonds of the chitosan in addition to N–H stretching of pure PANI [30–32,35]. The band located at $2,916\text{ cm}^{-1}$ was assigned to stretching of –CH group [30,40]. The characteristic band around $1,709\text{ cm}^{-1}$ was assigned to the overlap of –C=O, –NH stretching of the secondary amide of chitosan [30,41–43]. The main chain characteristic bands of polyaniline located at $1,601$ and $1,416\text{ cm}^{-1}$ were attributed to the C=N and C=C stretching modes for the quinoid and benzenoid rings, respectively [31,37,38]. The band appeared at $1,269\text{ cm}^{-1}$ due to C–N stretching vibration of PANI [31,39,42]. The peaks at $1,094$ and $1,060\text{ cm}^{-1}$ attributed to asymmetric stretching of the C–O–C of chitosan saccharide ring and the skeletal vibration of C–O stretching of PVA, respectively [43]. The band at 817.85 cm^{-1} is assigned to C–H out-of-plane bending vibration of 1,4-disubstituted benzene ring [31,37]. The peak located at 630.7 cm^{-1} was assigned to bending vibration –OH group [30]. For the FTIR spectrum after adsorption of AB 25, the PANI after adsorption had its C–H stretching at about $2,360\text{ cm}^{-1}$. Some C=O and C=C groups were found at $1,644$ and $1,733\text{ cm}^{-1}$ wave numbers; the presence of some amines and nitro functional groups was located on peak numbers

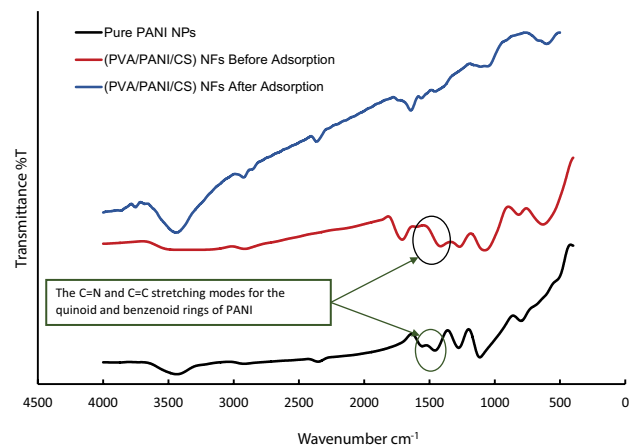


Fig. 5. FTIR spectra of polyaniline nanoparticles and the optimized PVA/CS/PANI composite nanofibers.

$1,465\text{ cm}^{-1}$ (NH₂ stretching), $1,562\text{ cm}^{-1}$ (NO₂ asymmetric stretching) and $1,150\text{ cm}^{-1}$ (saturated secondary amine C–N stretch), respectively, which were attributed to the AB 25 adsorbed onto PANI-based NFs. It was found also that band intensities that support the adsorption of dye molecules onto the pores of PANI composite were decreased after the adsorption [44].

3.3.4. Thermal gravimetric analysis

Fig. 6 investigates the comparison between the thermal gravimetric analysis (TGA) thermograms of the prepared PANI nanoparticles and the optimized PANI-based nanofibers; three stages of weight loss are observed for pure PANI. PANI starts a slow decomposition since the beginning of the test because of the evaporation of the compounds with low molar weights such as water [45]. PANI shows high moisture loss due to hygroscopic nature [46]. A very small weight loss about 11.7% is observed in the temperature range of $100\text{--}375.5\text{ }^{\circ}\text{C}$ due to degradation of the dopant (HCl) [46,47], followed by continuous losses in the temperature range from $375.5\text{ }^{\circ}\text{C}$ to $599.7\text{ }^{\circ}\text{C}$ with maximum loss about 31.8%. This weight loss is attributed to the decomposition as well as degradation of the polymer [47,48]. While the TGA thermogram of the optimized PANI-composite nanofibers shows three main stages of weight loss, PANI composite starts a slow decomposition since the beginning of the test at $25.2\text{ }^{\circ}\text{C}$ till $222.6\text{ }^{\circ}\text{C}$ because of the evaporation of the compounds with low molar weights such as water and the dopant HCl [45]. The maximum weight loss is observed in the temperature range of $222.6\text{--}390.8\text{ }^{\circ}\text{C}$ due to the structure decomposition of polyvinyl alcohol [48,49]; the final weight losses of about 25.4% are noticed in the temperature range from $390.8\text{ }^{\circ}\text{C}$ to $599.6\text{ }^{\circ}\text{C}$ that attributed to the degradation of polyaniline in addition to the degradation of saccharide structure of chitosan [47,48,51].

3.3.5. Surface area analysis

Surface area analysis has a key role in the adsorption phenomenon. The surface areas of the prepared nanofiber

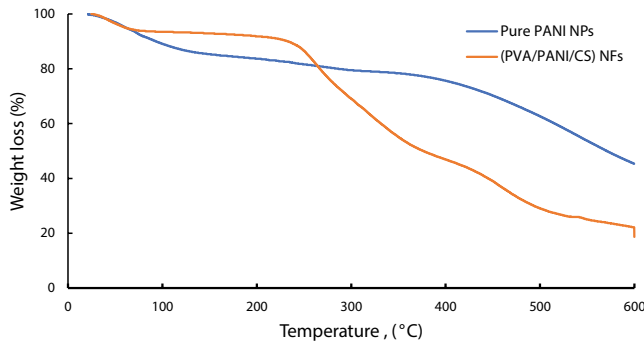


Fig. 6. Thermogram of the prepared PANI nanoparticles and the optimized PANI nanofibers.

composites before and after adsorption of AB dye were determined by adsorption–desorption of nitrogen gas through BET method. The obtained results showed that the surface areas of PANI-based nanofiber before adsorption process is 57.759 m²/g; while after adsorption of AB, the surface areas decreased to 32.608 m²/g. The decrease in surface areas after adsorption of dye confirms the adsorption process [52].

3.4. Adsorption of acid blue 25 onto the optimized prepared PANI-based NFs

3.4.1. Effect of contact time and initial dye concentration

As shown in Fig. 7, the % removal of different initial dye concentrations (10, 30, 50, 70 mg/L) using the prepared PANI-based NFs was plotted against the time. It was indicated that the dye removal increases with time and attains equilibrium at about 60 min for the concentrations 10 and 30 mg/L. While 90 min is the equilibrium time for the solutions of concentrations 50 and 70 mg/L. It was observed that after equilibrium, the dye uptake reached a constant value of about 90%, where at this point the amount of dye being adsorbed on the polymer is in a state of dynamic equilibrium with the amount of dye desorbed [53]. The dye uptake was rapid at the beginning of the adsorption process due to the presence of large amount of active sites on the adsorbent surface, thus dye could interact with these sites easily. After reaching the equilibrium time, saturation of the active sites on the adsorbent surface occurs. So, there is no considerable change in dye removal [30].

The equilibrium time is also dependent on the initial concentrations of dye. Specifically, the time to reach equilibrium increases from 60 to 90 min with an increase in initial concentration from 10 to 70 mg/L. This behavior may be due to the primary stages of adsorption, a large numbers of free adsorption sites are available on the adsorbent surface; however, as time passes, these sites are occupied by dye molecules and the adsorption capacity remains constant after equilibrium [38]. Hence, a contact time of 60 min was selected as the optimum removal time for the further experiments.

The adsorption kinetics for dye removal was investigated using the pseudo-first-order and pseudo-second-order kinetic models, which can be expressed by the following equations, respectively:

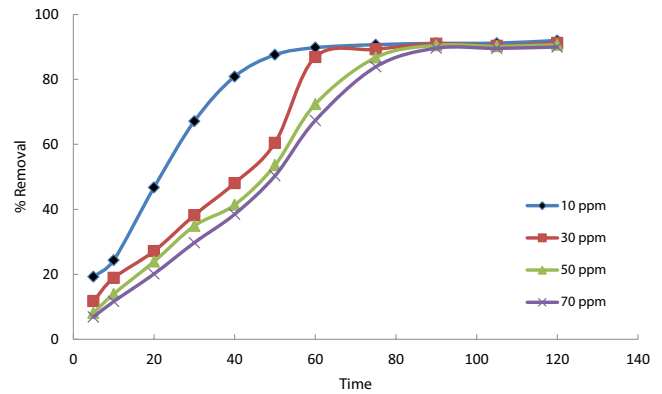


Fig. 7. Effect of contact time and initial dye concentration on the AB 25 removal by using the optimized PANI-based NFs.

$$\ln(q_e - q_t) = \ln q_e - k_1 t \quad (3)$$

$$\frac{t}{q_t} = \frac{1}{k_2 q_e^2} + \frac{t}{q_e} \quad (4)$$

where q_e and q_t are the amounts of AB 25 (mg/g) adsorbed at equilibrium and at time t (min), respectively, k_1 (1/min) is the adsorption rate constant of pseudo-first-order kinetic model and k_2 (g/mg min) is the pseudo-second-order rate constant [38,53–55]. Fig. 8a, showed the linear plotting of $\ln(q_e - q_t)$ vs. (t) , the rate constant k_1 and the value q_e for AB 25 removal can be determined graphically. While by plotting t/q_t vs. (t) according to Eq. (4), a straight line is obtained with slope $(1/q_e)$ and intercept $(1/k_2 q_e^2)$ as shown in Fig. 8b. The calculated parameters of the two kinetic models are tabulated in Table 1.

As shown in Table 1, the adsorption kinetics data of acid blue 25 on the best prepared PANI-based composite nanofibers are in agreement with the pseudo-first-order model, where the values of correlation coefficients, R^2 , are found to be all greater than 0.96 for all the studied concentrations.

3.4.2. Adsorption isotherms

The sorption isotherm models are fundamental to investigate the mechanism of adsorption. The Langmuir, Freundlich and Temkin isotherm models are widely used to describe the interactive behavior between the adsorbate and the adsorbent [30,56,57]. The linear form of Langmuir, Freundlich and Temkin isotherm equations can be expressed as follows:

Langmuir isotherm:

$$\frac{C_e}{q_e} = \frac{1}{K_L q_m} + \frac{C_e}{q_m} \quad (5)$$

Freundlich isotherm:

$$\ln q_e = \ln K_f + \frac{1}{n_f} \ln C_e \quad (6)$$

Temkin isotherm:

$$q_e = \frac{RT}{b_t} \ln A_t + \frac{RT}{b_t} \ln C_e \tag{7}$$

where C_e (mg/L) is the equilibrium dye concentration, q_e (mg/g) is the amount of dye adsorbed at equilibrium, q_m (mg/g) is the maximum adsorption capacity and K_L (L/mg) is the Langmuir equilibrium constant which indicates the nature of adsorption [58]. K_f (L/g) and n_f are the Freundlich constants related to the adsorption capacity and the adsorption intensity, respectively [30,59]. A_t (L/g) is the Temkin adsorption potential which represents the adsorbate–adsorbent interaction and related to the maximum binding energy, b_t (J/mol) is constant related to the heat of sorption, R is the ideal gas constant (8.314 J/mol K) and T is the temperature (K) [27,55]. The three isotherm models were graphically

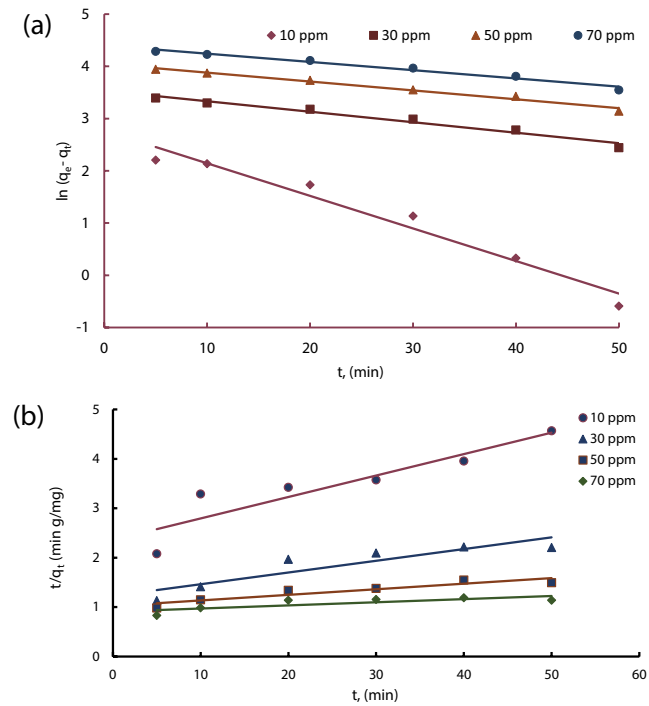


Fig. 8. (a) Pseudo-first-order and (b) pseudo-second-order kinetic graphs for the adsorption of AB 25 onto the prepared PANI-based composite NFs.

represented in Fig. 9, the isotherm parameters can be determined in Table 2. The Langmuir parameters q_m value was about 431.89 mg/g indicating excellent adsorption capacity for the fabricated PANI-based composite nanofibers.

From the Freundlich parameters, the value $n_f = 1.077$ is more than unity which means that the adsorption of AB 25 onto the prepared PANI-composite nanofibers is a favorable sorption process.

Comparing the correlation coefficients of the three sorption isotherm models Langmuir, Freundlich and Temkin, it was indicated that Freundlich model is the perfect model for describing the adsorption of AB 25 onto PANI composite

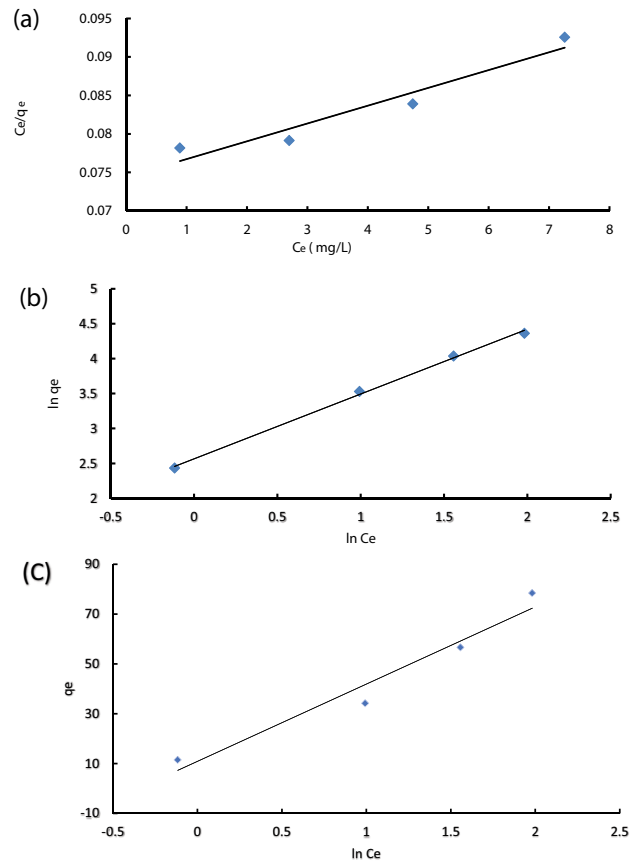


Fig. 9. (a) Langmuir, (b) Freundlich and (c) Temkin adsorption isotherm graph for AB 25 sorption by using the optimized PANI NFs.

Table 1
Pseudo-first-order and pseudo-second-order kinetic parameters for adsorption of AB 25

Experimental		Pseudo-first-order			Pseudo-second-order		
Initial AB 25 Conc. (mg/L)	q_e experimental (mg/g)	k_1 (min^{-1})	q_e calculated (mg/g)	R^2	k_2 (g/mg min)	q_e calculated (mg/g)	R^2
10	11.50	0.0623	15.93	0.9635	7.97×10^{-4}	23.05	0.8365
30	34.20	0.0201	34.26	0.9710	4.59×10^{-4}	42.19	0.8196
50	56.69	0.0170	57.44	0.9828	1.27×10^{-4}	87.79	0.8602
70	78.75	0.0158	81.45	0.9761	4.36×10^{-5}	158.86	0.6395

Table 2
Isotherm parameters for AB 25 sorption by using the optimized PANI composite nanofibers

	R^2	0.928
Langmuir	q_m (mg/g)	431.89
	K_L (L/mg)	0.0311
Freundlich	R^2	0.997
	n_f	1.077
	K_f (L/g)	13.011
Temkin	R^2	0.952
	b_t (J/mol)	79.93
	A_t (L/g)	1.42

nanofibers indicating excellent fitting of adsorption data to Freundlich model for heterogenous multilayer sorbent.

3.4.3. Effect of temperature

As shown in Fig. 10, the adsorption capacity of PANI-based NFs for AB 25 increases with increasing the temperature increase, proving that the sorption process is endothermic, where the temperature increases the diffusivity of dye particles [38].

3.4.4. Thermodynamic studies

The change in standard free energy (ΔG°), standard enthalpy change (ΔH°), and standard entropy change (ΔS°) of adsorption were calculated from the following equations [60,61]:

$$\Delta G^\circ = -RT \ln K_c \tag{8}$$

$$K_c = \frac{C_A}{C_S} \tag{9}$$

where ΔG° is the standard free energy change (kJ/mol), R is the universal gas constant (8.314 J/mol K), K_c is the equilibrium constant and T is the temperature in K and C_A and C_S are the equilibrium concentrations of dye on adsorbent (mg/g) and in the solution (mg/L), respectively [59,60]:

The free energy (ΔG°) for the specific sorption is calculated by using the following equations [59,60]:

$$\Delta G^\circ = \Delta H^\circ - T\Delta S^\circ \tag{10}$$

$$\ln K_c = \frac{\Delta S^\circ}{R} - \frac{\Delta H^\circ}{RT} \tag{11}$$

where ΔH° and ΔS° are the standard enthalpy change (kJ/mol) and the standard entropy change (kJ/mol K), respectively. ΔH° and ΔS° can be determined graphically from the van't Hoff plot of ($\ln K_c$) vs. ($1/T$), as shown in Fig. 11, where the slope and intercept of this plot equals to $-\Delta H/R$ and $\Delta S/R$, respectively [60,61].

The calculated thermodynamic parameters obtained are summarized in Table 3. The calculated negative values of

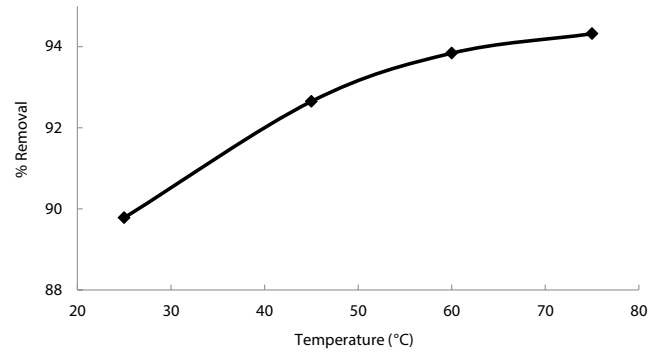


Fig. 10. Effect of temperature on the AB 25 removal by using the prepared PANI-based composite NFs.

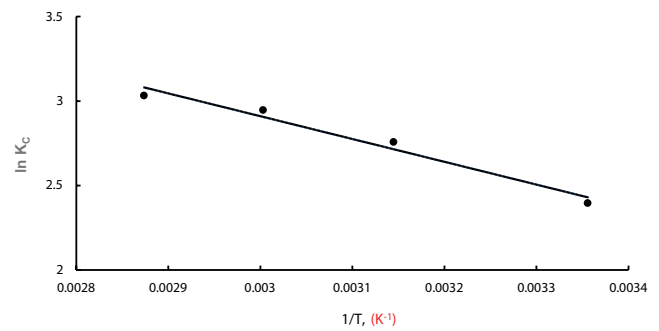


Fig. 11. van't Hoff plot of $\ln K_c$ against $1/T$ for AB 25 adsorption by using the optimized PANI NFs.

Table 3
Thermodynamic parameters of the adsorption of AB 25 onto the optimized prepared PANI-based composite nanofibers

Temperature (K)	ΔG° (kJ/mol)	ΔH° (kJ/mol)	ΔS° (kJ/mol K)
298	-6.022	11.212	0.058
318	-7.178		
333	-8.046		
348	-8.913		

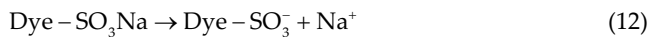
ΔG° indicate the feasibility and spontaneous nature of the sorption processes under standard conditions. It is also observed that ΔG° becomes more negative with raising temperature, confirming greater sorption at higher temperatures [42,57,61–63]. The positive value of enthalpy change ΔH° confirms that the adsorption process is endothermic. The value of ΔH° could give information about the type of adsorption. The magnitude of ΔH° for physisorption is 2.1–20.9 kJ/mol and for chemisorption is 20.9–418.4 kJ/mol [30,47,48,50]. The ΔH° value of this adsorption process equals to 11.212 kJ/mol for PANI composite nanofibers, indicating that the adsorption process is physisorption process. The positive value of ΔS° reflects the affinity of the adsorbent material for AB 25 as well as increase of randomness at solid–solution interface during dye adsorption [42,60,61,63].

3.4.5. Effect of pH

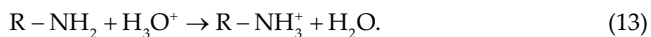
Solution pH has a great effect on acid blue 25 removal with inhibition observed at high pH values as shown in Fig. 12. The acid blue 25 decolorization by PANI-based nanofibers kept nearly 80% in the pH range of 3.0–7.0. Further increase of the solution pH above 7.0, the removal decreased to about 49% at pH 9.0 and the lowest % dye removal was observed at pH 11.0 [56,57].

This could be explained by the fact that at low pH, amine groups of polyaniline and chitosan are easily protonated, which induces an electrostatic attraction between dye molecules and adsorption sites, while at high pH more OH⁻ ions are available to compete with the anionic sulfonic groups of acid blue 25 for the adsorption sites of polyaniline and chitosan. This phenomenon decreases the number of adsorption sites for acid blue 25 [57].

The mechanism of this electrostatic attraction can be explained as following. Dye molecules in aqueous solution dissociated as:



In acidic pH, the amino group of the prepared composite protonated as:



As a final point, the adsorption process incomes through the electrostatic attraction between the two counter ions (positively charged nitrogen atom and the dye anion; Fig. 13).



Finally, by comparing the dye-adsorption performance of PANI-composite nanofibers with other adsorbents which is widely used in practice, we could find that PANI-composite nanofiber prepared in the present work provides a higher maximum adsorption capacity Q_{max} . The term maximum adsorption capacity Q_{max} (mg/g) was introduced (the amount adsorbed per mass of adsorbent) to compare between the produced PANI-composite nanofibers and other adsorbent used for removal of AB 25. Fig. 14 shows a plot of Q_{max} for different adsorbents and the created PANI-composite nanofibers. According to this term, Noby et al. [64] studied the

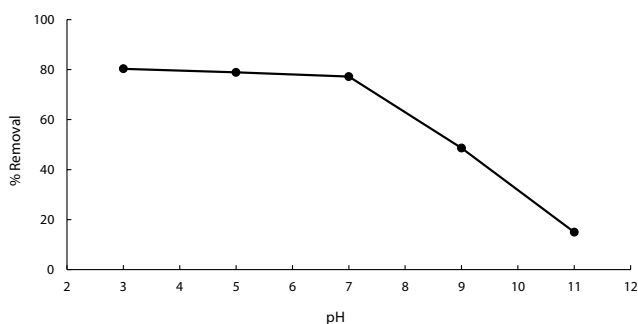


Fig. 12. Effect of pH on the AB 25 removal by using the optimized PANI composite NFs.

adsorption of AB 25 onto different morphologies of synthesized polyaniline nanorods and nanoparticles with maximum dye adsorption capacity Q_{max} of the two nanostructured materials 78 and 70 mg/g, respectively, has studied the correlation between the adsorption capacity of commercial activated carbons and the pore size distributions in the removal of anionic dyes such as AB 25 where the maximum dye adsorption capacity Q_{max} was found to be 345 mg/g [65]. Jiang et al. [43] studied the preparation of waste tea activated carbon through chemical activation with a novel activating agent potassium acetate and using it for the sorption of AB 25 and the maximum dye adsorption capacity Q_{max} was found 203.34 mg/g. In the present work, PANI-composite nanofibers manifested $Q_{\text{max}} = 431.89$ mg/g. Therefore, an efficient adsorption process could be developed with the created PANI nanostructures.

4. Conclusion

The characteristics of PANI represented in the crystalline nature and thermal stability make it a good choice to be electrospun and used in many applications. However, pure PANI has low electrospinnability, blending it with other polymers such as CS and PVA has a great potential for electrospinning uniform PANI-based NFs with low diameters. The novelty in this work for the electrospinning of PANI easily through using mixture of solvents, namely, DMF for

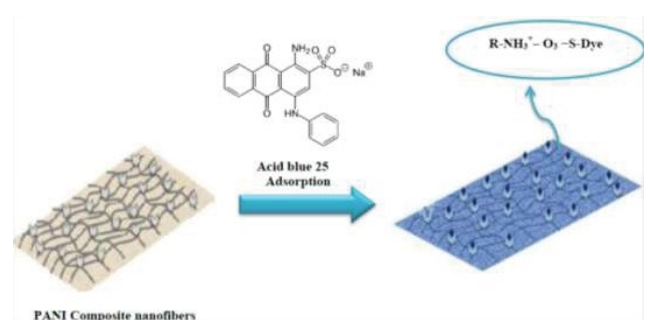


Fig. 13. Interactions of Acid blue dye with PANI-based nanofibers.

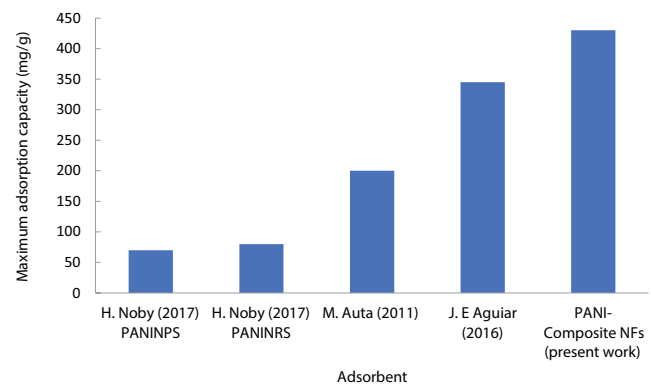


Fig. 14. Plot of Q_{max} of AB 25 adsorption for different adsorbents and the created PANI-composite nanofibers.

dispersing PANI NPs and water for dissolving the other polymers (PVA and CS), where the increase of PANI concentration was found to decrease the nanofibers diameters, also the addition of chitosan was noticed to decrease the diameters of nanofibers and make the electrospinning process easier. The prepared NFs were found to have high thermal stability, which make them available for use at high temperatures for many applications such as decolorization of wastewater contaminated with AB 25. These NFs showed high adsorption capacity for acidic dyes such as AB 25. By studying the parameters of AB 25 adsorption onto the optimum PANI-based NFs, it was found that the process is physisorption, endothermic and spontaneous. Also, it was observed that at high pH more OH⁻ ions will be available to compete with the anionic sulfonic groups of AB 25 for the adsorption sites of polyaniline and chitosan and the removal inhibition occurs.

References

- [1] G. Sharma, A. Kumar, M. Naushad, A. Kumar, A.a.H. Al-Muhtaseb, P. Dhiman, A.A. Ghfar, F.J. Stadler, M.R. Khan, Photoremediation of toxic dye from aqueous environment using monometallic and bimetallic quantum dots based nanocomposites, *J. Clean. Prod.*, 172 (2018) 2919–2930.
- [2] A. Kumar, A. Kumar, G. Sharma, A.a.H. Al-Muhtaseb, M. Naushad, A.A. Ghfar, C. Guo, F.J. Stadler, Biochar-templated g-C₃N₄/Bi₂O₃CO₃/CoFe₂O₄ nano-assembly for visible and solar assisted photo-degradation of paraquat, nitrophenol reduction and CO₂ conversion, *Chem. Eng. J.*, 339 (2018) 393–410.
- [3] M. Naushad, M. Ali Khan, Z. Abdullah Allothman, M. Rizwan Khan, M. Kumar, Adsorption of methylene blue on chemically modified pine nut shells in single and binary systems: isotherms, kinetics, and thermodynamic studies, *Desal. Wat. Treat.*, 57 (2015) 15848–15861.
- [4] Y. Liu, G. Zeng, L. Tang, Y. Cai, Y. Pang, Y. Zhang, G. Yang, Y. Zhou, X. He, Y. He, Highly effective adsorption of cationic and anionic dyes on magnetic Fe/Ni nanoparticles doped bimodal mesoporous carbon, *J. Colloid Interface Sci.*, 448 (2015) 451–459.
- [5] G. Zeng, Y. Liu, L. Tang, G. Yang, Y. Pang, Y. Zhang, Y. Zhou, Z. Li, M. Li, M. Lai, X. He, Y. He, Enhancement of Cd(II) adsorption by polyacrylic acid modified magnetic mesoporous carbon, *Chem. Eng. J.*, 259 (2015) 153–160.
- [6] J.L. Gong, B. Wang, G.M. Zeng, C.P. Yang, C.G. Niu, Q.Y. Niu, W.J. Zhou, Y. Liang, Removal of cationic dyes from aqueous solution using magnetic multi-wall carbon nanotube nanocomposite as adsorbent, *J. Hazard. Mater.*, 164 (2009) 1517–1522.
- [7] A.B. Albadarin, M.N. Collins, M. Naushad, S. Shirazian, G. Walker, C. Mangwandi, Activated lignin-chitosan extruded blends for efficient adsorption of methylene blue, *Chem. Eng. J.*, 307 (2017) 264–272.
- [8] M. Naushad, S. Vasudevan, G. Sharma, A. Kumar, Z.A. Allothman, Adsorption kinetics, isotherms, and thermodynamic studies for Hg²⁺ adsorption from aqueous medium using alizarin red-S-loaded amberlite IRA-400 resin, *Desal. Wat. Treat.*, 57 (2015) 18551–18559.
- [9] R. Ullah, G.A. Bowmaker, C. Laslau, G.I.N. Waterhouse, Z.D. Zujovic, K. Ali, A.-U.-H.A. Shah, J. Travas-Sejdic, Synthesis of polyaniline by using CuCl₂ as oxidizing agent, *Synth. Metals*, 198 (2014) 203–211.
- [10] K. Parashar, N. Ballav, S. Debnath, K. Pillay, A. Maity, Hydrous ZrO₂ decorated polyaniline nanofibres: synthesis, characterization and application as an efficient adsorbent for water defluoridation, *J. Colloid Interface Sci.*, 508 (2017) 342–358.
- [11] G. Sharma, A. Kumar, K. Devi, S. Sharma, M. Naushad, A.A. Ghfar, T. Ahamad, F.J. Stadler, Guar gum-crosslinked-Soya lecithin nanohydrogel sheets as effective adsorbent for the removal of thiophanate methyl fungicide, *Int. J. Biol. Macromol.*, 114 (2018) 295–305.
- [12] A. Sionkowska, Current research on the blends of natural and synthetic polymers as new biomaterials: review, *Prog. Polym. Sci.*, 36 (2011) 1254–1276.
- [13] K. Sharma, V. Kumar, B.S. Kaith, V. Kumar, S. Som, S. Kalia, H.C. Swart, Synthesis, characterization and water retention study of biodegradable Gum ghatti-poly(acrylic acid–aniline) hydrogels, *Polym. Degrad. Stabil.*, 111 (2015) 20–31.
- [14] G. Sharma, A. Kumar, M. Naushad, A. Garcia-Penas, A.H. Al-Muhtaseb, A.A. Ghfar, V. Sharma, T. Ahamad, F.J. Stadler, Fabrication and characterization of Gum arabic-cl-poly(acrylamide) nanohydrogel for effective adsorption of crystal violet dye, *Carbohydr. Polym.*, 202 (2018) 444–453.
- [15] G. Sharma, M. Naushad, D. Pathania, A. Kumar, Multifunctional nanocomposite pectin thorium(IV) tungstomolybdate for heavy metal separation and photoremediation of malachite green, *Desal. Wat. Treat.*, 57 (2015) 19443–19455.
- [16] V. Thavasi, G. Singh, S. Ramakrishna, Electrospun nanofibers in energy and environmental applications, *Energy Environ. Sci.*, 1 (2008) 205–221.
- [17] C. Feng, K.C. Khulbe, T. Matsuura, S. Tabe, A.F. Ismail, Preparation and characterization of electro-spun nanofiber membranes and their possible applications in water treatment, *Sep. Purif. Technol.*, 102 (2013) 118–135.
- [18] L. Zhang, T. Menkhaus, H. Fong, Fabrication and bioseparation studies of adsorptive membranes/felts made from electrospun cellulose acetate nanofibers, *J. Membr. Sci.*, 319 (2008) 176–184.
- [19] S. Schneiderman, L. Zhang, H. Fong, T.J. Menkhaus, Surface-functionalized electrospun carbon nanofiber mats as an innovative type of protein adsorption/purification medium with high capacity and high throughput, *J. Chromatogr. A.*, 1218 (2011) 8989–8995.
- [20] Q.P. Pham, U. Sharma, A.G. Mikos, Electrospinning of polymeric nanofibers for tissue engineering applications: a review, *Tissue Eng.*, 12 (2006) 1197–1211.
- [21] Z. Dong, S.J. Kennedy, Y. Wu, Electrospinning materials for energy-related applications and devices, *J. Power Sources*, 196 (2011) 4886–4904.
- [22] R. Gopal, S. Kaur, Z. Ma, C. Chan, S. Ramakrishna, T. Matsuura, Electrospun nanofibrous filtration membrane, *J. Membr. Sci.*, 281 (2006) 581–586.
- [23] R.J. Beck, Y. Zhao, H. Fong, T.J. Menkhaus, Electrospun lignin carbon nanofiber membranes with large pores for highly efficient adsorptive water treatment applications, *J. Water Process Eng.*, 16 (2017) 240–248.
- [24] M.S. Zoromba, S. Alghool, S.M.S. Abdel-Hamid, M. Bassyouni, M.H. Abdel-Aziz, Polymerization of aniline derivatives by K₂Cr₂O₇ and production of Cr₂O₃ nanoparticles, *Polym. Adv. Technol.*, 28 (2017) 842–848.
- [25] G. Sharma, B. Thakur, M. Naushad, A. Kumar, F.J. Stadler, S.M. Alfadul, G.T. Mola, Applications of nanocomposite hydrogels for biomedical engineering and environmental protection, *Environ. Chem. Lett.*, 16 (2017) 113–146.
- [26] A.M. Abd El-aziz, A. El-Maghraby, N.A. Taha, Comparison between polyvinyl alcohol (PVA) nanofiber and polyvinyl alcohol (PVA) nanofiber/hydroxyapatite (HA) for removal of Zn²⁺ ions from wastewater, *Arab. J. Chem.*, 10 (2017) 1052–1060.
- [27] M. Matouq, N. Jildeh, M. Qtaishat, M. Hindiyeh, M.Q. Al Syouf, The adsorption kinetics and modeling for heavy metals removal from wastewater by *Moringa* pods, *J. Environ. Chem. Eng.*, 3 (2015) 775–784.
- [28] B. Wessling, Conductive Polymer/Solvent Systems: Solutions or Dispersions?, in: *Handbook of Nanostructured Materials and Nanotechnology*, 2000, pp. 769–778.
- [29] A. Rose, N. Raghavan, S. Thangavel, B. Uma Maheswari, D.P. Nair, G. Venugopal, Investigation of cyclic voltammetry of graphene oxide/polyaniline/polyvinylidene fluoride nanofibers prepared via electrospinning, *Mater. Sci. Semicond. Proc.*, 31 (2015) 281–286.
- [30] X. Jiao, Y. Gutha, W. Zhang, Application of chitosan/poly(vinyl alcohol)/CuO (CS/PVA/CuO) beads as an adsorbent material for the removal of Pb(II) from aqueous environment, *Colloids Surf., B*, 149 (2017) 184–195.

- [31] M.M. Ayad, N.A. Salahuddin, I.M. Minisy, W.A. Amer, Chitosan/polyaniline nanofibers coating on the quartz crystal microbalance electrode for gas sensing, *Sensor Actuat. B*, 202 (2014) 144–153.
- [32] M.I. Voronova, O.V. Surov, S.S. Guseinov, V.P. Barannikov, A.G. Zakharov, Thermal stability of polyvinyl alcohol/nanocrystalline cellulose composites, *Carbohydr. Polym.*, 130 (2015) 440–447.
- [33] A. Alakanandana, A.R. Subrahmanyam, J. Siva Kumar, Structural and electrical conductivity studies of pure PVA and PVA doped with Succinic acid polymer electrolyte system, *Mater. Today: Proceedings*, 3 (2016) 3680–3688.
- [34] M.R. Karim, Fabrication of electrospun aligned nanofibers from conducting polyaniline copolymer/polyvinyl alcohol/chitosan oligosaccharide in aqueous solutions, *Synth. Met.*, 178 (2013) 34–37.
- [35] R.E. Morsi, E.A. Khamis, A.M. Al-Sabagh, Polyaniline nanotubes: Facile synthesis, electrochemical, quantum chemical characteristics and corrosion inhibition efficiency, *J. Taiwan Inst. Chem. Eng.*, 60 (2016) 573–581.
- [36] J. Tang, X. Jing, B. Wang, F. Wang, Infrared spectra of soluble polyaniline, *Synth. Met.*, 24 (1988) 231–238.
- [37] Y. Li, X. Zhao, Q. Xu, Q. Zhang, D. Chen, Facile preparation and enhanced capacitance of the polyaniline/sodium alginate nanofiber network for supercapacitors, *Langmuir*, 27 (2011) 6458–6463.
- [38] M. Bhaumik, R.I. McCrindle, A. Maity, S. Agarwal, V.K. Gupta, Polyaniline nanofibers as highly effective re-usable adsorbent for removal of reactive black 5 from aqueous solutions, *J. Colloid Interface Sci.*, 466 (2016) 442–451.
- [39] A. Chellachamy Anbalagan, S.N. Sawant, Brine solution-driven synthesis of porous polyaniline for supercapacitor electrode application, *Polym. J.*, 87 (2016) 129–137.
- [40] M. Ayad, G. El-Hefnawy, S. Zaghlool, Facile synthesis of polyaniline nanoparticles; its adsorption behavior, *Chem. Eng. J.*, 217 (2013) 460–465.
- [41] Y. Gutha, J.L. Pathak, W. Zhang, Y. Zhang, X. Jiao, Antibacterial and wound healing properties of chitosan/poly(vinyl alcohol)/zinc oxide beads (CS/PVA/ZnO), *Int. J. Biol. Macromol.*, 103 (2017) 234–241.
- [42] R. Karthik, S. Meenakshi, Facile synthesis of cross linked-chitosan-grafted-polyaniline composite and its Cr(VI) uptake studies, *Int. J. Biol. Macromol.*, 67 (2014) 210–219.
- [43] M. Jiang, K. Wang, J.F. Kennedy, J. Nie, Q. Yu, G. Ma, Preparation and characterization of water-soluble chitosan derivative by Michael addition reaction, *Int. J. Biol. Macromol.*, 47 (2010) 696–699.
- [44] M. Auta, B.H. Hameed, Preparation of waste tea activated carbon using potassium acetate as an activating agent for adsorption of Acid Blue 25 dye, *Chem. Eng. J.*, 171 (2011) 502–509.
- [45] Z. Qiang, G. Liang, A. Gu, L. Yuan, Hyperbranched polyaniline: a new conductive polyaniline with simultaneously good solubility and super high thermal stability, *Mater. Lett.*, 115 (2014) 159–161.
- [46] S. Bilal, S. Gul, R. Holze, A.-u.-H.A. Shah, An impressive emulsion polymerization route for the synthesis of highly soluble and conducting polyaniline salts, *Synth. Met.*, 206 (2015) 131–144.
- [47] P.S.R. Devi, M.N. Deo, S. Kawadiya, N. Raje, S.R. Vishwakarma, R. Verma, A.V.R. Reddy, Evaluation of the effect of heating on the ion exchange capacity of polyaniline, *Synth. Met.*, 210 (2015) 297–303.
- [48] L. Ding, X. Wang, R.V. Gregory, Thermal properties of chemically synthesized polyaniline (EB) powder, *Synth. Met.*, 104 (1999) 73–78.
- [49] C. Santos, C.J. Silva, Z. Buttel, R. Guimaraes, S.B. Pereira, P. Tamagnini, A. Zille, Preparation and characterization of polysaccharides/PVA blend nanofibrous membranes by electrospinning method, *Carbohydr. Polym.*, 99 (2014) 584–592.
- [50] Z. Peng, L.X. Kong, A thermal degradation mechanism of polyvinyl alcohol/silica nanocomposites, *Polym. Degrad. Stabil.*, 92 (2007) 1061–1071.
- [51] S. Kumari, S.H. Kumar Annamareddy, S. Abanti, P. Kumar Rath, Physicochemical properties and characterization of chitosan synthesized from fish scales, crab and shrimp shells, *Int. J. Biol. Macromol.*, 104 (2017) 1697–1705.
- [52] S. Xuan, F. Wang, J.M. Lai, K.W. Sham, Y.X. Wang, S.F. Lee, J.C. Yu, C.H. Cheng, K.C. Leung, Synthesis of biocompatible, mesoporous Fe₃O₄ nano/microspheres with large surface area for magnetic resonance imaging and therapeutic applications, *ACS Appl. Mater. Inter.*, 3 (2011) 237–244.
- [53] R.E. Morsi, M.Z. Elsabee, Polyaniline nanotubes: mercury and competitive heavy metals uptake, *Am. J. Polym. Sci.*, 5 (2015) 10–17.
- [54] F. Hayeeye, M. Sattar, W. Chinpa, O. Sirichote, Kinetics and thermodynamics of Rhodamine B adsorption by gelatin/activated carbon composite beads, *Colloids Surf., A*, 513 (2017) 259–266.
- [55] S.A. Chaudhry, Z. Zaidi, S.I. Siddiqui, Isotherm, kinetic and thermodynamics of arsenic adsorption onto iron-zirconium binary oxide-coated sand (IZBOCS): modelling and process optimization, *J. Mol. Liq.*, 229 (2017) 230–240.
- [56] J. Wang, K. Zhang, L. Zhao, Sono-assisted synthesis of nano-structured polyaniline for adsorption of aqueous Cr(VI): effect of protonic acids, *Chem. Eng. J.*, 239 (2014) 123–131.
- [57] A. Kamari, W.S.W. Ngah, M.Y. Chong, M.L. Cheah, Sorption of acid dyes onto GLA and H₂SO₄ cross-linked chitosan beads, *Desalination*, 249 (2009) 1180–1189.
- [58] A.E. Chávez-Guajardo, J.C. Medina-Llamas, L. Maqueira, C.A.S. Andrade, K.G.B. Alves, C.P. de Melo, Efficient removal of Cr (VI) and Cu (II) ions from aqueous media by use of polypyrrole/maghemite and polyaniline/maghemite magnetic nanocomposites, *Chem. Eng. J.*, 281 (2015) 826–836.
- [59] L. Tang, Y. Fang, Y. Pang, G. Zeng, J. Wang, Y. Zhou, Y. Deng, G. Yang, Y. Cai, J. Chen, Synergistic adsorption and reduction of hexavalent chromium using highly uniform polyaniline-magnetic mesoporous silica composite, *Chem. Eng. J.*, 254 (2014) 302–312.
- [60] H.M. Gad, A.A. El-Sayed, Activated carbon from agricultural by-products for the removal of Rhodamine-B from aqueous solution, *J. Hazard. Mater.*, 168 (2009) 1070–1081.
- [61] R. Kumar, M.O. Ansari, M.A. Barakat, DBSA doped polyaniline/multi-walled carbon nanotubes composite for high efficiency removal of Cr(VI) from aqueous solution, *Chem. Eng. J.*, 228 (2013) 748–755.
- [62] M.A. Shaker, H.M. albishri, Dynamics and thermodynamics of toxic metals adsorption onto soil-extracted humic acid, *Chemosphere*, 111 (2014) 587–595.
- [63] C. Sun, C. Li, C. Wang, R. Qu, Y. Niu, H. Geng, Comparison studies of adsorption properties for Hg(II) and Au(III) on polystyrene-supported bis-8-oxyquinoline-terminated open-chain crown ether, *Chem. Eng. J.*, 200–202 (2012) 291–299.
- [64] H. Noby, A. El-Shazly, M. Elkady, M. Ohshima, Adsorption Profiles of Acid Dye Using Synthesized Polyaniline Nanostructure with Different Morphologies, *J. Chem. Eng. Jpn.*, 50 (2017) 170–177.
- [65] J.E. Aguiar, J.C.A. de Oliveira, P.F.G. Silvino, J.A. Neto, I.J. Silva, S.M.P. Lucena, Correlation between PSD and adsorption of anionic dyes with different molecular weights on activated carbon, *Colloids Surf.*, 496 (2016) 125–131.